

(Abstract)

Line 14. “rates” -> “values” ?

**Reply:** We modify to ratios of overlap area between two eddies to the area of each eddy.

Line 15. “temporarily” (spelling).

**Reply:** suggestion followed.

Lines 19-20. “. . the number N of look-ahead time steps, and . .”

**Reply:** suggestion followed.

Line 20. I Googled “computational complexity” . I think the number of operations (which is what you count) is one aspect of computational complexity but might be better described as number of operations.

**Reply:** Yes, computational complexity here refers to time complexity, i.e., the number of operations. We now used *time complexity* hereafter. The computational time of the algorithm is detailed in section 5.4.

(1 Introduction)

Lines 55, 426, 430 (and maybe other places) “noise” not “noises” .

**Reply:** thank you.

Line 60. Something missing at “. . is [Chelton . .”

**Reply:** we modified to ‘. . it is a solution to the “missing eddy” problem [Chelton . .’

Line 63. Omit “following”

**Reply:** suggestion followed.

(2.1 Input data)

Line 118. “detection, . .”

**Reply:** thank you.

Line 120. Omit “to”

**Reply:** suggestion followed.

Line 127. “territories” -> “areas”. [You said you would use “areas”. “territory” suggests land, not sea. Especially, if “. . and boundaries” then “areas” is the word. “areas and boundaries” might be “territories” on land; “domains” is the mathematical word.

**Reply:** suggestion followed.

(3.1 Overview of GEM)

Line 205. “. . In addition to eddy area and boundary, . . input, the critical values of area ratio  $r_c$  and N. See section 5.2 . . .” (duplication of “input” ).

**Reply:** suggestion followed.

(3.2 Map link)

Line 210. Maybe “territory” -> “domain”

**Reply:** suggestion followed.

Lines 217, 218, 219, 226. Maybe likewise “territories” -> “domains”. For all these “area” is also possible but less precise.

**Reply:** suggestion followed.

Line 221. “B2 only had partial similarity” . B1 is discussed but not B2. Also not obvious in

figure.

**Reply:** We had used 19970328 and 19970329 in the first time (and the description text was also for such dates), but incorrectly used 19970301 and 19970302 in the last time. Now we redraw the figures with 19970328 and 19970329.

Lines 237-238. I think you need to say here, how the values of  $r_1$  and  $r_2$  decide whether it is T1 or T2. See lines 262-263 for how  $r_2$  determines T1; this should be at line 238.

**Reply:** suggestion followed.

Line 274. “(section 3.4)”

**Reply:** thank you.

Line 275. “. . . similar, and 2) the earliest day. Rule 1 . . .” (i.e. omit “first” twice, it is confusing).

**Reply:** suggestion followed.

Lines 276, 282. “E1” -> “Ed1” .

**Reply:** suggestion followed.

Line 283. “. . . as the following Ed2, Ed3 respectively.” ?

**Reply:** suggestion followed.

(3.3 Track tree)

Lines 304, 305. Again you should say how the values of  $r_1$  and  $r_2$  decide whether it is “first type” or “second type” .

**Reply:** criteria have been added.

(4.1 Eddy tracks)

Lines 356-357. “Eddy C1 . . . trajectory is the longest” . This is a good reason for choosing it as the only example; it has the best chance of showing any problem! You should say this and also that you did actually look at many others.

**Reply:** Yes! We pointed out that in the above paragraph.

Line 371. “it” - not clear what this refers to.

**Reply:** Sorry for that. We modified “it” to “the application of similarity vector”.

(5.2 Impact of variations of parameters)

Lines 447-448. Maybe better “To discuss the impact of the GEM critical value  $r_c$  and look-ahead time  $N$ , we carry out . . . 2012. The number of eddies”

**Reply:** suggestion followed.

Line 474. “O-W” needs defining here (bring definition from lines 498-9).

**Reply:** suggestion followed.

Line 474 “sensitive” . What is sensitive to what? I think you perhaps mean that “suitable  $r_c$  depends on whether it is O-W or SLA identification” .

**Reply:** Yes. GEM based on Okubo–Weiss (O–W) parameter identification O-W based identification is much sensitive to the critical value  $r_c$ .

Line 481. “to though” . This does not make sense and I cannot say what you do mean!

**Reply:** Sorry for that. It has been modified

Lines 496-497. Better “comparison of eddies identified by different methods, since the eddy detection algorithms differ a lot from each other.” ?

**Reply:** suggestion followed.

Figure 4. This is OK on my screen but had dark infill when I printed it; please check.

**Reply:** We redraw the figure with light colors.

Figure 6. There is no illustration of T1.

**Reply:** Yes, there is no T1 in the figure, since there is at most one eddy that can be marked as a T1 (merging) or T3 (living) eddy on the following day (section 3.2.2). We add this notation to the label of figure.

Line 692. “. . (b) There are four similarity types . .”

**Reply:** suggestion followed.

# GEM: A Dynamic Tracking Model for Mesoscale Eddies in the Ocean

Qiu-Yang Li<sup>1</sup>, Liang Sun<sup>1, 2</sup>, Sheng-Fu Lin<sup>1</sup>

<sup>1</sup>School of Earth and Space Sciences, University of Science and Technology of China, 230026, Hefei, China.

<sup>2</sup>State Key Laboratory of Satellite Ocean Environment Dynamics, Second Institute of Oceanography, State Oceanic Administration, Hangzhou, 310012, PR China.

Correspondence to: L. Sun ([sunl@ustc.edu.cn](mailto:sunl@ustc.edu.cn))

## Abstract

Genealogical Evolution Model (GEM) is an efficient logical model used to track dynamic evolution of mesoscale eddies in the ocean. It can distinguish different dynamic processes (e.g., merging and splitting) within a dynamic evolution pattern, which is difficult to accomplish using other tracking methods. To this end, GEM first uses a two-dimensional (2-D) similarity vector (i.e. a pair of ~~overlap rates~~ ratios of overlap area between two eddies to the area of each eddy) rather than a scalar to measure the similarity between eddies, which effectively solves the “missing eddy” problem (~~temporally temporarily~~ lost eddy in tracking). Second, GEM uses both parents (a new eddy) and children (e.g., splitting eddies from parent eddy) in tracking, and the dynamic processes are described as birth and death of different generations. Additionally, a look-ahead approach with selection rules effectively simplifies computation and recording. All of the computational steps are linear and do not include iteration. Given the pixel number of the target region  $L$ , the maximum number of eddies  $M$ , ~~the look-ahead time steps  $N$~~  the number  $N$  of look-ahead time steps, and the total number of time steps  $T$ , the total ~~computation time~~ complexity is  $O(LM(N+1)T)$ . The tracking of each eddy is very smooth because we require that the snapshots of each eddy on adjacent days overlap one another.

Although eddy splitting or merging is ubiquitous in the ocean, they have different geographic distribution in the Northern Pacific Ocean. Both the merging and splitting rates of the eddies are high, especially at the western boundary, in currents and in “eddy deserts.” GEM is useful not only for satellite-based observational data but also for numerical simulation outputs. It is potentially useful for studying dynamic processes in other related fields, e.g., the dynamics of cyclones in meteorology.

带格式的: 字体: 倾斜

## 30 1 Introduction

31 Eddies are ubiquitous in the ocean, and they move from one place to another [Chelton and Schlax, 1996; Chelton et  
32 al., 2007]. Eddies in the ocean can cause large-scale transports of heat, salt and other tracers [Bennett and White,  
33 1986; Chelton et al., 2011a; Dong et al., 2014; McGillicuddy et al., 2011] by trapping these passive tracers inside the  
34 eddies. Such transports may have important impacts on the environment and climate of the ocean [Dong et al., 2014].  
35 To address various applications in the studies that use satellite products of sea level anomaly (SLA) data [e.g.,  
36 Chelton et al., 2011b] and numerical simulation outputs [e.g., Petersen et al., 2013], oceanic eddies should be  
37 automatically recorded using these data and outputs [e.g., Yang et al., 2013; Sun et al., 2014; Pegliasco et al., 2015].  
38 In general, the recording of oceanic eddies often includes two independent steps: automated eddy identification and  
39 automated eddy tracking. The eddies are identified in a sequence of SLA maps using an identification algorithm or  
40 identified from velocity fields. An automated tracking procedure is then applied to determine the trajectory of each  
41 eddy [Chelton et al., 2011b]. Several automated identification and tracking algorithms have been developed for  
42 eddies in the ocean [Chelton et al., 2011b; Ienna et al., 2014; Mason et al., 2014; Yi et al., 2015].

43 For the eddy tracking stage, according to a recent census [Wang et al., 2015; Yi et al., 2015], approximately 10-30%  
44 of eddies may be found in proximity to a neighboring eddy in any given global SLA map and they frequently  
45 interact. Therefore, an eddy tracking process should have the capability to distinguish different dynamic processes  
46 (e.g., merging and splitting) during its dynamic evolution. Moreover, an eddy tracking process must be accurate and  
47 fast enough to handle a huge amount of data, which will be even larger in size if spatio-temporal resolution of  
48 observations and numerical simulations increases.

49 Implemented automated tracking procedures differ in detail, but they are all similar in concept because they utilize  
50 the nearest neighbor strategy [Chelton et al., 2011b]. For each eddy  $E_i$  identified at time step  $k$ , the nearest eddy to  $E_i$   
51 at the next time step  $k+1$  is identified as part of the trajectory of eddy  $E_i$ . A more advanced procedure uses eddy  
52 shape error as an additional condition when assessing an eddy trajectory [Mason et al., 2014].

53 However, there is a “missing eddy” problem that must be solved in the eddy tracking stage [Chelton et al., 2011b].  
54 An eddy at time step  $k$  may have no associated eddy at time step  $k+1$ , which is simply due to a temporary missing  
55 eddy in the identification process; this can occur for a variety of reasons related to sampling errors and measurement  
56 ~~noises-noise~~ [Chelton et al., 2011b] or limitations of the eddy detection step when an eddy is too weak/small at a  
57 time step. Chelton and his colleagues made an attempt to accommodate such problems; they allowed for the  
58 reappearance of a temporarily missing eddy by looking ahead two or three time steps. Unfortunately, this “look-  
59 ahead” procedure considers too many nearby eddies as potential ones. In practice, the results of this simple “look-  
60 ahead” procedure were disappointing because the resulting eddy ~~trajectory-trajectories~~ often jumped from one eddy  
61 track to another. As a result, the look-ahead approach was abandoned, even though it is [a solution to the “missing](#)  
62 [eddy” problem](#) [Chelton et al., 2011b].

63 Recently, the concept of Multiple Hypothesis Assignment (MHA) was introduced to solve the missing eddy problem  
64 by abandoning the simple closest eddy strategy and applying a new “look-ahead” procedure [Faghmous et al., 2013].

65 | The MHA method can effectively solve the missing eddy problem in a straight-line model when the following  
66 | trajectory being followed is a branch without any splitting, but it is algorithmically and computationally complex.  
67 | Given the maximum number of eddies in any time frame  $M$ , the number of look-ahead time steps  $N$  (with  $N=0$  being  
68 | the original linear closest eddy procedure without look-ahead) and the total number of time steps  $T$ , the MHA has a  
69 | larger computational-time complexity (the total amount of time taken by an algorithm),  $O(M^{N+1}T)$  at the worst-case  
70 | [Faghmous et al., 2013].

71 | The existing straight-line model can trace the kinematic motion of eddy. The dynamic evolutionary processes (e.g.,  
72 | merging and splitting) of the eddy are, however, ignored by the model. This implies that each eddy  $E_i$  identified at  
73 | time step  $k$  has only one eddy as part of its trajectory at time step  $k-1$  and has only one eddy as part of its trajectory  
74 | at time step  $k+1$ . In the ocean, small eddies may merge to form larger ones. As shown in Figure 1, the anticyclonic  
75 | eddies AC1 and AC2 observed on July 26, 2006 merged into a single one on July 31, 2006. Then, the cyclonic  
76 | eddies C1 and C2 on July 26, 2006 merged to form a larger one on August 3, 2006. To describe such processes, the  
77 | eddy tracking records should be trees with branches instead of simple straight lines.

78 | To record the dynamic evolution of eddies, two fundamental algorithms are required. First, the two nearby eddies  
79 | should be distinguished in the identification stage using a segmentation strategy in which the target region is divided  
80 | into two corresponding eddies. Otherwise, the merging and splitting processes cannot be determined properly. This  
81 | problem was recently solved by the use of segmentation strategies, e.g., the close-distance segmentation strategy [Li  
82 | et al., 2014] and the watershed strategy [Li and Sun, 2015]. Because these segmentation strategies can distinguish  
83 | closed eddies, they can also potentially reduce the risk of having a missing eddy in the identification process.

84 | Second, the merging and splitting processes in the tracking stage should be described in detail. We use a multi-  
85 | branch tree model to do so. The eddy  $E_i$  identified at time step  $k$  may arise from more than one eddy at time step  $k-1$ ,  
86 | which subsequently merged; and  $E_i$  may become more than one eddy at time step  $k+1$  if it splits. We refer to this  
87 | model as the “Genealogical Evolution Model (GEM)” because it is a genealogical tree for recording the whole  
88 | evolutionary history of an eddy. The multi-way tree model in computer science can be used to store this type of  
89 | structure.

90 | Moreover, the GEM also provides a new way to solve the missing eddy problem. Instead of the existing closest eddy  
91 | strategy, a temporal track tree with  $N$  look-ahead time steps is used to maintain all possible tracks with the help of  
92 | the multi-way tree model. The method can effectively solve the missing eddy problem, regardless of whether the  
93 | eddy is splitting or not.

94 | In this paper, we introduce the GEM to describe mesoscale eddies in a tracking process with a total number of time  
95 | steps  $T$ . The GEM allows the eddy to have multiple eddies as its parents or as its children in a multi-branch model. It  
96 | also solves the missing eddy problem by using a new look-ahead method similar to the MHA. Compared with the  
97 | computational-time complexity  $O(M^{N+1}T)$  of MHA, the new method is much faster and has much less  
98 | computational-time complexity  $O(LM(N+1)T)$ , where  $L$  denotes the pixels of target region. Besides, if the GEM  
99 | was implemented with the computer codes properly, the output data of GEM also record the dynamic evolution of

100 the eddy in detail and will potentially be useful for other research fields, e.g., the dynamics of cyclones in  
101 meteorology. As an example, The GEM is applied to eddies in the North Pacific Ocean (NPO) only, and we assume  
102 the eddies do not cross the equator.

103 The paper is organized as follows. The data and eddy detection methods used in this study are introduced in section  
104 2. Then GEM is introduced in section 3, including similarity vector, look-ahead approach and the worst-case  
105 runtime complexity i.e. ~~computational-time~~ complexity. Results including eddy tracks and examples of merging and  
106 splitting events in a sample area in the North Pacific are shown in section 4. The impacts of data noise and  
107 parameters uncertainties on the results are discussed in section 5. Finally, a summary and conclusions are given in  
108 section 6.

109

## 110 2 Eddy identification

### 111 2.1 Input data

112 The input data consists of the original altimetry field, which can come from satellite observations or numerical  
113 simulations. The altimetry field used in this study is the 20-year (1993-2012) daily SLA data from the merged and  
114 gridded satellite product of Maps of Sea Level Anomaly (MSLA) at  $0.25^\circ \times 0.25^\circ$  resolution in the global ocean  
115 from AVISO (<http://www.aviso.oceanobs.com/>). In this study, we use the “DT14” (delayed-time 2014) altimeter  
116 product [Duacs/AVISO, 2014], which is adequate for direct eddy detection [Capet et al., 2014] though it still has  
117 about 2-3 cm error globally for short temporal scales [Carrere et al., 2016]. A comprehensive discussion of gridded  
118 Aviso products for eddy investigations can be found in Chelton et al. (2011b).

119 We used the original SLA data (“DT14”) without any filtering or smoothing to identify eddies in this study.  
120 However, this does not imply that data smoothing is not needed for the SLA data in related studies (e.g. eddy  
121 ~~detection~~detection, eddy tracking). For example, to calculate some eddy parameters (e.g., velocity and vorticity),  
122 smoothing may be required, as pointed out by Chelton et al. (2011b). Moreover, the data errors, even if they are very  
123 small, might affect ~~to~~ the eddy detection (see discussion in section 5.1).

### 124 2.2 Eddy identification

125 The eddy identification used in this study is similar to those used before [Chelton et al., 2011b; Mason et al., 2014],  
126 to identify eddies from SLA data. The eddies may be identified with multinuclear (two or more SLA extremes in  
127 one eddy) or mononuclear (only one SLA extremum in one eddy). The following mononuclear eddy definition is also  
128 similar to what was used by other authors [Chaigneau et al., 2011; Li et al., 2014; Li and Sun, 2015]. We have  
129 adopted the eddy detection step from Li and Sun (2015), which provides us with the necessary input for the tracking  
130 routines, namely eddy ~~territories~~areas and boundaries. Each pixel has eight nearest neighbours. A point within the  
131 region is a local extremum if it has an SLA greater or less than all of its nearest neighbours. We also use such  
132 definition of extremum in our following analysis, in which the extrema are identified by checking each pixel in the

133 map along with the eight pixels around it. An eddy is defined as a simply-connected set of pixels that satisfies the  
134 following criteria:

- 135 (1) The SLA value of all of the pixels is above (below) a given SLA threshold;
- 136 (2) Only *one* SLA extremum exists in the pixel set;
- 137 (3) The amplitude of the eddy (the max difference of SLA values) is larger than a critical value (e.g., 1 cm);
- 138 (4) The area of the eddy must be large enough for estimating eddy parameters (say >16 pixels).

139 Conditions (3)-(4) provide the lower bounds for eddy size and amplitude. These conditions automatically reduce the  
140 total number of detected eddies. Condition (1) is the same as the first [criteria-criterion](#) in Chelton et al., (2011b). It is  
141 used in consideration of the 2-3 cm of background SLA error [Carrere et al., 2016]; so, small fluctuations in SLA  
142 field would not be taken as eddies in this study. Condition (3) was generally used previously [Chaigneau et al., 2011;  
143 Chelton et al. 2011]. Condition (4) is more restrictive than the generally used value of eight pixels [e.g., Chelton et  
144 al., 2011; Li et al., 2014]; so, this condition is an add-on, which is potentially useful when deriving eddy parameters  
145 using a nonlinear optimal fitting method [Wang et al., 2015; Yi et al., 2015]. If the eddy area is too small (only a few  
146 pixels), its parameters (e.g. amplitude, area, radius, etc.) are very sensitive to its area (number of pixels). Besides, we  
147 don't put limits on eddy pixel number maximum (e.g., <1000) and eddy size (e.g., <400-1200 km) while such limits  
148 were generally used previously [e.g., Chelton et al. 2011; Mason et al., 2014].

149 The SLA extremum so determined is called eddy center. The set of pixels belonging to an individual eddy is referred  
150 to as the area of the eddy, and the outmost SLA contour is the boundary of the eddy. We use the area and boundary  
151 to calculate the similarity of eddies in section 3.2.

152 Each eddy is identified by the following procedures. First, according to condition (1), we find a simply-connected  
153 region with a given threshold of  $SLA > 3$  cm for cyclonic eddies and  $SLA < -3$  cm for anticyclonic eddies. Second, we  
154 check whether there is at least one extremum in the region. If the eddy is multinuclear, we use a segmentation  
155 method to segment them to satisfy condition (2). Finally, we check whether the region satisfies the eddy conditions  
156 (3) and (4); we remove those weak (amplitude < 1 cm) and small (pixels < 16) eddies.

157

### 158 2.3 Eddy segmentation for merging and splitting events

159 Figure 2 illustrates the necessity for eddy segmentation based on the merging process of two eddies. Two different  
160 mononuclear algorithms are used in the upper and lower rows. In the top panels of Figure 2, eddies are identified by  
161 non-segmentation algorithm. Such mononuclear eddies may be very small. The time evolutions from  $t=1$  to  $t=3$   
162 show a decay scenario of two closed eddies C1 and C2. Both their amplitudes and areas become smaller and smaller  
163 with time. Then, a large eddy C3 suddenly appears in the same region without any premonition. It is hard to see  
164 what happened during the time from  $t=1$  to  $t=3$  from the parameters (amplitude and area) of mononuclear eddies



165 identified by reducing the number of contours of the SLA until there is only one extreme in the contour (Chaigneau  
166 et al., 2011) instead of the segmentation algorithm [Li and Sun, 2015]. In contrast, the bottom panels of Figure 2  
167 show a merging scenario of two closed eddies C1 and C2 using the segmentation algorithm [Li and Sun, 2015].  
168 During the time from  $t=1$  to  $t=2$ , both their amplitudes and areas are only marginally changed, while their distance is  
169 continually reduced. Then, a large eddy C3 naturally emerges in the same region, while C1 and C2 disappear. It is  
170 recognized from the eddy data that C3 is the merging result of C1 and C2.

171 Figure 3 illustrates this eddy segmentation strategy. Figure 3a shows two individual but nearby eddies. The pixels  
172 between the two dashed lines are naturally divided by the watershed (For basins, the “watershed” is a ridge between  
173 them, while it is a valley for plateaus). As shown in Fig. 3b, the cross section of the eddy clearly shows that two  
174 closely located pixels  $P_1$  and  $P_2$  on the left and right sides of watershed would slide along the path of steepest descent  
175 in the map of SLA data to different eddy centres. The shape of SLA can provide sufficient information to segment  
176 the multinuclear eddy into mononuclear ones.

177 Herein, we use the Mononuclear Eddy Identification (MEI) of the Universal Splitting Technology for Circulations  
178 (USTC) with watershed segmentation [Li and Sun, 2015] and include in our code the calculation of eddy  
179 parameters, including amplitude, radius, area, and boundary (Fig. 3), which might be potentially used in other  
180 studies [Sun et al., 2014].

181 The output eddy parameters from MEI is then used as input for our novel tracking algorithm GEM. The GEM  
182 mainly represents the logical relationship of eddies, which is less dependent on physical parameters which may  
183 change greatly because of dynamic evolution (e.g., splitting, merging). To this end, the GEM takes the previously  
184 identified eddies by MEI (with area/boundary, see section 2.2) as its input data.

185

### 186 **3 Dynamic tracking**

#### 187 **3.1 Overview of GEM**

188 The GEM is a logical model used for tracking the dynamic evolution of mesoscale eddies in the ocean (Fig. 4). The  
189 model essentially establishes logical relationships of previously identified eddies. The relationships are determined  
190 by two relatively independent steps i.e. the GEM algorithm consists of two parts (see Fig.4 for details): first,  
191 measuring the “map link” between two time steps and then connecting all time steps to the “track tree.”

192 The first part of GEM is “map link,” which uses as input eddy data obtained in the prior eddy identification step  
193 (area/boundary, see section 2.2) to establish the link of an eddy from one temporal snapshot to the next, namely  
194 living, missing, death, birth, and the associated dynamical processes of merging and splitting. In this part of the  
195 work flow, we use a 2-D vector rather than a passive scalar to measure the similarity between eddies  $E_1$  and  $E_2$  on  
196 two neighboring days (Figs. 5 and 6, see section 3.2.1 for details). We then use a relatively complex look-ahead

197 procedure to solve the missing eddy problem (section 3.2.2). This new look-ahead approach has a duration of  $N$  days  
198 (Fig. 7). Finally, the links of the eddies in different snapshots are saved (see section 3.2.2 for details).

199 The second part is “track tree,” which uses the outputs from “map link” (i.e., eddy links), as its input (Fig. 4). It  
200 connects the eddy links from branches to a tree with the genealogical model (Fig. 8) using two sub procedures:  
201 “eddy branch” and “eddy tree.” In the “eddy branch” part, we use *parent* and *child* to define the eddy relationship  
202 and define all possible types of eddy states: birth, death, living, missing, merging and splitting (Fig. 8a).  
203 Consequently, we identify different roles in the eddy branches (see section 3.3.1 for details). Finally, in the “eddy  
204 tree” procedure, we connect the branches based on their roles (parent, child, and grandchild, etc.) in the genealogical  
205 tree (Fig. 8b). The output of GEM includes eddy tracks and the records of eddy relationships (see section 3.3.2 for  
206 details).

207 In short, the GEM uses previously identified eddies and/or their links to make dynamic tracks via a genealogical tree  
208 model. In addition to eddy territory domain and boundary, it needs two parameters as input, it includes two  
209 parameters, the critical value of area ratio  $r_c$  and  $N_c$  as inputs. See section 5.2 for discussion on the impacts of these  
210 parameter choices.

## 211 3.2 Map link

212 To establish the relationships between the previously identified eddies, the first part of GEM used evaluates the  
213 similarity of these eddies which is defined here based on the overlap of the territory domain of an eddy in two  
214 consecutive time steps. It begins with defining similarity based on the overlapping area of eddies in consecutive time  
215 steps. Subsequently, the overlapping area which is closest to the one of the original eddy is defined to be the  
216 successor of the original eddy (if the threshold is met).

### 217 3.2.1 Eddy similarity

218 At first, the eddy similarity is calculated with an example (Fig. 5a) before proceeding to the mathematical  
219 expressions. There were three eddies A1, A2 and B1 detected on March 28, 1997. In Figure 5b, there were four  
220 eddies, A1, A2, B1, and B2 on March 29, 1997. We overlapped the eddy territories domains into a single map (Fig.  
221 5c). Then, we used the intersection of eddy territories domains on different days to calculate the similarity. For  
222 eddies A1 and A2, the intersections were very close to their respective territories domains on March 28 and 29. For  
223 eddy B1, the intersection was close to the area on the second day, but it was only part of that on the first day.  
224 Consequently, eddies A1 and A2 had full similarity on these days, while eddies B1 and B2 only had partial  
225 similarity on these days.

226 To estimate the above similarity, let us describe it in a mathematically logical way. As shown in Figure 6a, there is  
227 an eddy ( $E_1$ ) that is identified by the thick contour of Boundary 1 in the rectangular comparison region (not shown in  
228 figure) on day 0, and there are three eddies ( $E_2$ ,  $E_3$  and  $E_4$ ) that are identified in the same region on day 1. This  
229 comparison region, which is centered at the eddy center of  $E_1$ , moves in time with the target eddy ( $E_1$ ). To determine

230 | the similarities between  $E_1$  on day 0 and  $E_2$  to  $E_4$  on day 1, we intersect the ~~territories-domains~~ of day 0 and day 1.  
 231 | For example, to determine the similarity between  $E_1$  and  $E_2$ , we count the overlap area  $S_{12}$  (defined as the  
 232 | intersection of Boundary 1 and Boundary 2) between  $E_1$  (area  $S_1$ ) and  $E_2$  (area  $S_2$ ), and then we calculate the  
 233 | following ratios:

$$234 \quad r_1 = S_{12} / S_1, \quad (1a)$$

$$235 \quad r_2 = S_{12} / S_2. \quad (1b)$$

236 | Clearly, the values of  $r_1$  and  $r_2$  are within  $[0,1]$ . The larger  $r_1$  and  $r_2$  are, the larger possibility that  $E_2$  has to be the  
 237 | snapshot of  $E_1$  on day 1. Eddy movement speeds are generally less than 0.1 m/s, which implies that an eddy can only  
 238 | move one grid box ( $0.25^\circ$ ) in 3-4 days. Thus, the overlap on different subsequent days of the same eddy area should  
 239 | be large enough. This is one of the parameters to set. When we applied GEM to track eddies in the Northern Pacific  
 240 | Ocean, we choose  $r_c=2/3$ , and the choice of  $r_c$  is comprehensively addressed in section 5.2.

241 | Using the vector  $(r_1, r_2)$  and the critical value  $r_c$ , we define four different types of similarity between two eddies (Fig.  
 242 | 6b). From low to high, they are as follows: Type 0 (T0:  $r_1 < r_c$  and  $r_2 < r_c$ ), where  $E_1$  and  $E_2$  are unrelated; Type 1 (T1:  
 243 |  $r_1 > r_c$  and  $r_2 < r_c$ ), where  $E_1$  on day 0 is part of  $E_2$  on day 1 ( $E_1$  enlarging or merging); Type 2 (T2:  $r_1 < r_c$  and  $r_2 > r_c$ ),  
 244 | where  $E_2$  on day 1 is part of  $E_1$  on day 0 ( $E_1$  decaying or splitting); and Type 3 (T3:  $r_1 > r_c$  and  $r_2 > r_c$ ), where  $E_1$  and  
 245 |  $E_2$  are the same eddy at different locations on different days ( $E_1$  living and moving). The last type (T3, living) is  
 246 | prescribed in cases when the center of  $E_1$  propagates less than a pixel toward that of  $E_2$ , because the eddy movement  
 247 | speed is physically less than one grid ( $0.25^\circ$ ) per day. For example, eddy B1 on March 29, 1997 in Figure 5b is  
 248 | simply assigned to T3 (living) even though  $r_1 < r_c$ . Eventually, we obtain the relationships between  $E_1$  and  $E_3$  or  $E_4$   
 249 | (Fig. 6a). Because the present method uses a vector to express eddy similarity, we call it the similarity vector. This is  
 250 | an alternative to scalar similarity parameters [e.g., Ienna et al., 2014; Mason et al., 2014].

251 | For example, as shown in Figure 6a, the high similarity between  $E_1$  and  $E_2$  over a critical value  $r_c$  (marked as T3  
 252 | (living) in Fig. 6b) suggests an evolution from  $E_1$  to  $E_2$ . This is similar for eddies  $E_1$  and  $E_3$ , but with a different  
 253 | splitting relationship (marked as T2 (splitting) in Fig. 6b). The relationship between eddies  $E_1$  and  $E_4$  is designated  
 254 | as “unrelated” because of the overlap in their ~~territories-areas~~ is small or zero. In other words, their overlap rates are  
 255 | below the critical value  $r_c$  (marked as T0 in Fig. 6).

256 | In previous eddy tracking studies, simple methods were used for weekly SLA data (delayed-time 2010), e.g., the  
 257 | closest distance between eddies [Chelton et al., 2011b; Yi et al., 2015], the closest angle between eddies [Zhang et  
 258 | al., 2014] and the dimensionless similarity scalar [Chaigneau et al., 2008; Mason et al., 2014]. There is always a risk  
 259 | of eddy jumping (from one track to another) in these methods, except for that of Pegliasco et al. (2015), who used  
 260 | intersections of eddy boundaries to find the continuing eddy. Compared to the previous tracking methods, we use a  
 261 | more robust technique to assess the relationship of eddies in subsequent time steps by using the overlap of their  
 262 | ~~territories-areas~~. In addition, we do not simply assign the continuing eddy using the similarity vector for the two  
 263 | adjacent days; rather, we try to solve the temporary missing eddy problem by looking ahead a few days.

### 264 3.2.2 Eddy Look-ahead

265 In contrast to the procedure used in Chelton et al. (2011b), we use a relatively complex look-ahead procedure. An  
266 example for a given eddy are shown in Figure 7a. In the upper row, both Ec1 and Ec2 take the same eddy Ec3 as  
267 their subsequent T1 type of eddy, which is a merging event (e.g., eddies C1 and C2 in Fig. 1). Since a T1 (merging)  
268 eddy has  $r_2 < r_c$  (intersection only takes a part of the eddy Ec3 on day 1), two or more eddies (e.g., Ec1 and Ec2) on  
269 day 0 could identify the same eddy (Ec3) as T1 eddy simultaneously on day 1. In the middle row, eddy E1 has two  
270 T2 (splitting) type of eddies (Ec2, Ec3) at the same time; this is a splitting event (e.g., eddies B1 and B2 in Fig. 5).  
271 In the lower row, eddy E1 has T2 (splitting) and T3 (living) types of eddies (respectively Ec2, Ec3) at the same time.  
272 Although there may be many possibilities for any given eddy, there is at most one eddy that can be marked as a T1  
273 (merging) or T3 (living) eddy on the following day (as  $r_l > r_c = 2/3$  holds).

274 This new look-ahead approach with  $N=2$  is shown in Figure 7b. After finishing the calculation of the following  
275 eddies on day 1, we continue to calculate eddies on the following days. At this preparation stage, it is similar to the  
276 MHA method with important modifications [Faghmous et al., 2013]. What makes this look-ahead procedure novel  
277 and efficient is that we use two simple rules to directly choose only one day's result for the following eddies. Thus,  
278 the procedure becomes linear without iteration, and it is much faster than the MHA, as discussed in the subsection  
279 on the ~~computation complexity~~time complexity (section ~~3-63.4~~).

280 The two selection rules are: 1) the most similar-~~first~~, and 2) the earliest day-~~first~~. Rule 1 has priority. We first choose  
281 the most similar eddy as the potential successor of ~~Ed1~~Ed1 according to their types. According to Figure 6b, T2  
282 (splitting) type eddy covers only part of the original eddy while T1 (merging) eddy covers most part of the original  
283 eddy. The similarity from low to high is  $T2 < T1 < T3$ . For example, if there is only one T3 (living) eddy in these days,  
284 we choose it as the potential one. However, if there is more than one day with the same type of eddies, we need an  
285 additional rule: the earliest day-~~first~~. For example, in the upper row of Figure 7b, there is one T3 (living) eddy on  
286 day 1, ~~there is and~~ one T3 (living) eddy on day 2, and there are two T2 (splitting) eddies on day 3. In this case, we  
287 choose day 1 as the following day and the T3 (living) eddy as the following ~~Ed1~~Ed1. In the middle and the lower rows,  
288 we choose day 2 and day 3 as the following days and the corresponding T3 (living) eddies as the following ~~Ed1~~Ed2,  
289 Ed3 respectively.

290

## 291 3.3 Track tree

### 292 3.3.1 Eddy branch

293 After having determined the next subsequent days and the relationship types between eddies based on the above  
294 process, we can now establish the branches of an eddy from one day to the next. Eddy branch describes the  
295 relationship between two eddies at two different time steps. To describe the GEM more precisely, we use *parent* and

296 *child* to identify the different roles that the eddy plays in eddy branches. There are three types of logical  
297 relationships used in GEM, as shown in Figure 8a.

298 The upper row shows a successor relationship: an eddy P on day 1 has only one successor (eddy P itself) on day 2.  
299 In this case, eddy P is allowed to be missing during day 1 and day 2. Additionally, eddy P will be recorded as death  
300 (black circle), if no successor eddy is found after  $N$  days.

301 In the middle row, two (or more) eddies merge into one. The first type includes principal and subordinate merging.  
302 A principal eddy  $P_1$  and a subordinate eddy  $P_2$  on day 1 merge into a larger eddy  $P_1$  on day 2, whereas  $P_2$  is recorded  
303 as death. This occurs when a large eddy meets and merges with a small eddy (e.g., C1 and C2 in Fig. 1). The  
304 anticyclonic eddies A1 and A2 in Fig. 11 also experience a similar process (see section 4.2 for details). The second  
305 type is coordinated merging. Two (or more) parent eddies  $P_1$  and  $P_2$  merge to produce a new child eddy C, and all of  
306 the parent eddies are recorded as death. This is because the similarity ~~was~~is not sufficiently high for either eddy to  
307 which the record of eddy C should be appended. There might be another choice by keeping parent eddies  $P_1$  and  $P_2$   
308 alive and appending the record of eddy C to both eddies. This choice artificially increases lifetimes of eddy P1 and  
309 P2 and leads to other tracking problems; so, we abandon it.

310 In the lower row, a parent eddy splits into several child eddies. The first type is principal and subordinate splitting. A  
311 parent eddy P splits into ~~ana~~a relatively large eddy P (itself, i.e. the similarity type is T3 between the two eddies) and  
312 a relatively small child eddy C (i.e. the similarity type between parent eddy P and child eddy C is a splitting  
313 relationship T2), which is recorded as birth. The second type is coordinated splitting. Two (or more) child eddies are  
314 born from the parent eddy P, which is then recorded as death. This occurs when all the similarity types between  
315 child eddies and parent eddy are type 2 (T2).

### 316 3.3.2 Eddy tree

317 Finally, the track tree is recorded by connecting the eddy branches (Fig. 8b). Track tree of an eddy records  
318 information of all the associated eddies (e.g., living, death, birth, merging and splitting, etc.) during its entire life.  
319 In this process, the role that an eddy plays in the track tree is considered. The first generation is the parent eddy (e.g.,  
320  $P_1$ ), the second generation is the child eddy (e.g.,  $C_1$ ) and the third generation is the grandchild eddy (e.g.,  $G_1$ ). The  
321 track tree uses the above eddy branches (Fig. 8a). We connect the branches from one time to another to obtain the  
322 whole eddy track tree.

323 There are two additional notations. First, an eddy emerging from the same family of eddies (e.g., two siblings  $C_2$  and  
324  $C_4$ ) will be recorded as a new family member (e.g., eddy  $C_5$ ). Second, an eddy merging from two different families  
325 of eddies (e.g.,  $C_1$  and  $P_2$ ) will be recorded as a new eddy  $N_1$ .

326 Although the model could have several generations, we only recorded two generations i.e. parent and child in this  
327 study due to the complexity of the output data structure and the computational-time complexity. However, we can  
328 indirectly track other generations using the relationships between them.

### 329 **3.4 Computation complexityTime complexity**

330 To calculate similarity vectors, we need to overlap two small regions around eddy E1. The total number of pixels in  
331 the rectangular comparison region is  $L$ . The computational time complexity of the similarity vector is  $O(L)$  for each  
332 day. If we use  $N$  look-ahead time steps to find the best choice, the computation complexity of the  
333 branches will be  $O(L(N+1))$  for one eddy. Because all of the steps are linear without iteration, given the maximum  
334 number of eddies in any time frame  $M$ , the number of look-ahead time steps  $N$  and the total number of time steps  $T$ ,  
335 the total computation complexity is  $O(LM(N+1)T)$ . The GEM algorithm can hardly be made any  
336 faster. When the number of look-ahead time steps  $N$  is more than one, the computation complexity  
337 is much faster than  $O(M^{N+1}T)$  of MHA.

338 For example, both  $L$  and  $M$  are approximately 1000, and  $N=2$  is used in the present study. The MHA method will  
339 require on the order of  $10^2$ - $10^3$  times more computational time than the present method; and the larger the value of  $N$ ,  
340 the more efficient the present method is. The look-ahead time  $N$  may be potentially as large as one week ( $N=6$ ), as  
341 noted in the following discussion. Thus, the present method is especially effective compared to the previously  
342 suggested methods when a long look-ahead time is required for poorly identified eddies.

343

## 344 **4 Results**

### 345 **4.1 Eddy tracks**

346 We first apply the MEI to detect the ocean eddies in the North Pacific Ocean (NPO) during 1993-2012. The eddy  
347 centers (SLA extrema of eddy snapshots) on each day are counted on each  $1^\circ \times 1^\circ$  grid. In general, anticyclonic eddies  
348 are significantly more frequent than cyclonic eddies. As shown in Figure 9a, the cyclonic eddies are mainly located  
349 in the western part of the NPO. For example, there are lots of cyclonic eddies east of Japan near the Kuroshio, which  
350 can also be seen from both Figure 1 and the results in section 5.1. In contrast, anticyclonic eddies are mainly located  
351 in the eastern part of the NPO (Fig. 9b). For example, the eddies are mainly anticyclones in the red box, which can  
352 also be seen from the results in section 4.2. In general, the eddies are ubiquitous in Figure 9c (about 50-70 eddies per  
353 year on each  $1^\circ \times 1^\circ$  grid), except that there are several regions where both types of eddies are relatively scarce. One  
354 of them is known as “eddy desert” (black box in Figure 9c) [Chelton et al., 2007]. The other region is the North  
355 Equatorial Current (NEC) (blue box in Figure 9c) [Hu et al., 2015]. Finally, we present in Figure 9d the ratio of  
356 difference of the numbers of cyclonic and anticyclonic eddies to the total number of eddies.

357 We apply the GEM to these eddies detected by MEI with  $r_c=2/3$  and  $N=2$ . In the NPO, there are a total of 60276  
358 eddies with lifetimes longer than 30 days. Among them, 37553 of the eddies are anticyclonic and 22723 are cyclonic.  
359 The tracks of long-lived eddies are plotted in Figure 10. In general, they are similar to those shown in previous  
360 studies [Chelton et al., 2011b]. There are 7290 anticyclonic and 3627 cyclonic eddies with lifetimes longer than 100  
361 days (Fig. 10a), and the ratio of anticyclonic to cyclonic eddies is approximately 2. The ratio is larger for eddy  
362 lifetimes greater than 400 days, which was also noted in previous studies [Chelton et al., 2011b; Xu et al., 2011].

363 Each track is very smooth because we require that the snapshots of eddies on different days overlap one another. We  
364 have done a visual evaluation of many long-lifetime eddy trajectories and the quality of the tracking results is  
365 reasonable. We will take the long-lived C1 in Figure 10b as an example.

366 Eddy C1 was first detected as an eddy initiated on September 14, 1995, with an extremum at 163.5°W, 10.5°N. It  
367 then travelled to the northwest and disappeared at 151.25°W, 20.5°N on March 11, 1997. Its trajectory is the longest  
368 that we have detected in the NPO (Fig. 10b). The trajectory is smooth, except for a sudden jump from 167.5°E to  
369 166.75°E (Fig. 10c) on July 31, 1996. The GEM algorithm did very well at whether we should connect the  
370 trajectories from before July 30, 1996 with that after July 31, 1996, into a single trajectory.

371 To clarify this, we plot the two SLA fields in Figure 10d. The SLA field on July 30, 1996 is plotted as contours. The  
372 eddy center is marked by a black cross at 167.5°E, 16.5°N. In contrast, the SLA field on July 31, 1996 is plotted in  
373 shading. The eddy center is marked by a red cross at 166.75°E, 17.25°N. The distance between the eddy extrema was  
374 larger than 100 km within a day. Although that distance is far beyond the criterion applied in standard eddy tracking  
375 routines [Mason et al., 2014; Yi et al., 2015], we can see from the SLA fields that they both indicated the same eddy,  
376 and that it was consistent with our approach to connect the trajectories into a single trajectory.

377 There may be no associated eddy can be identified at the next time step for an eddy at time step  $k$ , and it may be the  
378 result of eddies temporarily “disappearing” for a variety of reasons related to sampling errors and measurement  
379 noise [Chelton et al., 2011b]. The application of similarity vector and look-ahead procedure can effectively  
380 accommodate such problems and allow for the reappearance of temporarily “disappearing” eddy in the tracking  
381 procedure. In turn, [the application of similarity vector](#) reduces the usage of the look-ahead procedure. It is clear  
382 that the similarity expressed as a vector is better than that as scalar using simple distance.

## 383 4.2 Eddy merging and splitting

384 The trajectories provide evidence of dynamic evolution. The time evolution of a couple of anticyclonic eddies is  
385 depicted in Figure 11a, which implies a merging process occurring in the red boxes in Fig. 9. As shown in Figure  
386 11a, eddy A1 had a westward movement with a speed of 2.6 cm/s, and eddy A2 lingered near 133°W. Then, both  
387 eddies merged into one large eddy on April 23, 1997. That evolutionary process is clearly shown by the SLA fields  
388 (Figs. 11c-j). In Figure 11c, there were two anticyclonic eddies, A1 and A2, located at 132°W, 28.5°N. Eddy A1  
389 moved from east to west with a nearly constant speed of 2.6 cm/s, whereas eddy A2 had negligible zonal motion.  
390 They then rotated clockwise about each other with an average angular velocity of  $6 \times 10^{-7} \text{ s}^{-1}$ , as denoted by the blue  
391 arrows. Finally, they merged into the new large eddy A2 (see animation in supplement).

392 The SLA field shows that an eddy splitting process also occurred in the box the same time. The time evolutions of  
393 anticyclonic eddies B1, B2 and B3 are depicted in Figure 11b. At first, eddy B1 had a fast westward speed of 10.4  
394 cm/s. It then split into two eddies (B1 and B2) on March 29, 1997 (Fig. 6). Eddy B1 traveled at its original speed  
395 whereas eddy B2 lingered at its origin. Then, eddy B3 emerged at a location between B1 and B2 on April 9, 1997,  
396 which slowed down the speed of B1 to approximately 3.5 cm/s. After that, eddies B2 and B3 merged into a new

397 eddy B3 on April 19, 1997. In fact, similar to eddies A1 and A2, eddies B1 and B2 eventually merged into a new  
398 eddy on May 20, 1997 (not shown). The SLA maps in Figures 11c-j show more details that were not recorded by the  
399 eddy tracking data. Note that eddy B2 had a very short lifetime of 20 days but a complex dynamic process. If only  
400 long-term eddies (lifetime > 30 days) were saved, the corresponding evolutionary process might not be recorded  
401 properly.

402 It is expected that a pair of cyclonic eddies will have a counter-clockwise rotation in the Northern Hemisphere,  
403 which is known as the Fujiwhara effect for atmospheric cyclones [Fujiwhara, 1921]. When two cyclones are close  
404 enough, they will begin to orbit cyclonically (counter-clockwise in the Northern Hemisphere). Because the above-  
405 mentioned eddies are anticyclonic, they have opposing directions of rotation, which appear as two point vortices  
406 moving in circular paths about the center of vorticity in classical fluid dynamics [Batchelor, 1967].

#### 407 **4.3 Census of merging and splitting events**

408 To illuminate how often the merging and splitting processes occurred, we counted the total number of merging and  
409 splitting events on each  $1^\circ \times 1^\circ$  grid each year. The merging and splitting events were homogeneously distributed in  
410 the oceans, but in general were very few times each year per  $1^\circ \times 1^\circ$  grid element. The merging frequencies for  
411 cyclonic eddies and anticyclonic eddies are shown in Figure 12, which are similar to their splitting frequencies (not  
412 shown). The distribution pattern of merging frequencies for cyclonic eddies in Figure 12a, is very similar to that of  
413 cyclonic eddy centers in Figure 9a. In contrast, the merging frequency for anticyclonic eddies was larger along the  
414 west coast (Fig. 12b), whereas the anticyclonic eddy centers were located mainly in the east (Fig. 9b). Although  
415 merging and splitting events may occur anywhere in the ocean there is spatial variation in the number of events (Fig  
416 12c, d):

417 The first type of special region is the western boundary. It is known that the western boundary is a sink of eddy  
418 energy caused by the interaction with the bottom and lateral topography [Zhai et al., 2010]. It is also known as a  
419 “graveyard” for westward-propagating ocean eddies [Zhai et al., 2010; Chelton et al., 2011b]. The second type of  
420 special region is located in strong currents, including the Kuroshio Current, and the NEC [Hu et al., 2015]. Among  
421 those currents, the eddies in the NEC had the highest frequency of merging and splitting events, which was not  
422 noted in previous studies. The third type of special region is located in the northeast Pacific, which is also known as  
423 an “eddy desert” [Chelton et al., 2007]. The fourth type of special region is located in enclosed marginal seas,  
424 especially the Bering Sea.

425 By comparing Figure 12 with Figure 10, we can see that the regions with high frequencies of merging and splitting  
426 events have relatively few eddy tracks, especially in the NEC (blue box in Figure 9c) and in the “eddy desert” (black  
427 box in Figure 9c) in the northeast Pacific. The existence of “eddy desert” may be due to the fact that the eddy was  
428 too small to be detected or the fact that the eddy lifetime was too short [Chelton et al., 2011b]. However, Figures 9  
429 and 12 suggest that merging and splitting events may be a major contributor to the “eddy desert”.



430 We also calculate the average dynamic (merging and splitting) events per eddy as a function of lifetime (Figure 13).  
431 The results are similar regardless eddy polarizations and dynamic types. The merging and splitting events are  
432 approximately linear increase with eddy lifetime. However, the anticyclonic eddies seem more vigorous in ocean  
433 dynamics than cyclonic eddies.

434

## 435 5 Discussion

### 436 5.1 Data ~~noises~~noise

437 Although “the Aviso product DT14” is much better than previous products, there are still some notable errors,  
438 especially for short temporal scales of less than two months [Carrere et al., 2016]. It was reported that there are  
439 along-track SLA errors of about 2-3 cm globally and of more than 3 cm at high latitudes and in shallow waters.

440 To reduce the ~~noises~~noise in SLA data, one may use the Gaussian structure filter [Chelton et al., 2011b; Mason et  
441 al., 2014], Hanning filters [Penven et al., 2005], or Lanczos filter [Chaigneau et al., 2008]. As certain parameters  
442 need to be chosen in these filters, the filtered results depend much on these parameters [see Fig. A1 in Chelton et al.,  
443 2011b]. As sensitivity test we apply a simple five-point quadratic smoothing to the SLA data. The filtered data are  
444 then piecewise  $C^2$ -smoothed by a quadratic function, which satisfies the potential requirements for calculating  
445 vorticity (second derivative of SLA) from SLA data.

446 Figure 14 shows the non-smoothed and smoothed SLA data from January 1, 1993 to January 4, 1993. The smoothed  
447 SLA maps are very close to the non-smoothed SLA maps. And the values at the SLA extrema (not shown) are close  
448 to their original values. This implies that the noise in the DT14 data is sufficiently small for our purpose.

449 However, the ~~noises~~noise cannot be neglected, even when they are small. They might induce additional SLA  
450 extrema (see the definition of extremum in section 2.2), which eventually affect eddy detection, e.g., the additional  
451 extremum on January 2, 1993 in box A and the additional extremum on January 3, 1993 in box B (Figure 14). These  
452 additional extrema existed only for a very short period (one or two days). But they can induce additional merging  
453 and splitting events, which may cause eddies to unexpectedly terminate [Chelton et al., 2011b]. The ambiguity of the  
454 eddy identification procedure, which may be caused by sampling errors and measurement noise in the input SLA  
455 data, strongly suggest the application of a look-ahead approach.

### 456 5.2 Impact of variations of parameters

457 To discuss the impact of ~~parameters  $N$  and  $r_c$~~ the GEM critical value  $r_c$  and look-ahead time  $N$ , we carry out a  
458 sensitivity study in the north Pacific from year 1993 to 2012. ~~There are two parameters in the GEM: the critical~~  
459 ~~value  $r_c$  and the look-ahead time  $N$ .~~The number of eddies with lifetimes  $> 30$  days is counted for different  $r_c$  and  $N$ ,  
460 as shown in Figure 15a. Note that the results are very similar, except for  $N=0$  (i.e., without any look-ahead). It is  
461 from the above discussion that we see look-ahead is necessary when there are extrema due to small ~~noises~~noise in

462 the data. The number of eddies does not change substantially with  $r_c$  for any  $N > 1$ , when  $r_c$  is within 0.5 to 0.8 (e.g.  
463 63469 eddies were identified with  $N=2$ ,  $r_c=0.5$  and the identified eddies number was 63630 with  $N=4$ ,  $r_c=0.8$ ).  
464 Meanwhile, the numbers of merging and splitting events are also counted for different  $r_c$  and  $N$ , as shown in Figure  
465 15b. In general, the splitting events occurs slightly more frequently than the merging events (e.g. 151220 splitting  
466 events and 150612 merging events for  $N=2$ ,  $r_c=0.5$ ). Note also that the results are very similar, except for  $N=0$ . The  
467 numbers of merging and splitting events seem to converge for  $r_c > 0.5$  as  $N$  increases. For each  $N > 0$ , the numbers of  
468 merging and splitting events reach a maximum at  $r_c=0.6$ . A relatively loose similarity condition ( $r_c < 0.5$ ) will lead to  
469 a risk of eddy jumping from one track to another, which consequently reduces both total eddy number and dynamic  
470 events. On the other hand, a relatively strict similarity condition ( $r_c > 0.9$ ) will lead to a risk of missing eddies, which  
471 may also reduce both total eddy numbers and dynamic events.

472 In general, one would like the tracking results to be insensitive to the choice of these parameters. From Figure 15,  
473 we can observe that  $0.5 < r_c < 0.8$  appears to be a choice with relatively robust results. The optimal value for  $r_c$  might  
474 be 0.6-0.7, which is reasonable. In one hand, we first require that  $r_c > 0.5$ . On the other hand, we know there is area  
475 error in calculation (~10%) since only eddy grids are taken into consider. This is also the reason why we need  $r_c$   
476  $< 0.9$  or even smaller. So the optimal value should be within 0.5-0.9, and ~0.7 is just in this middle. We also find that  
477 the look-ahead time  $N$  should be larger than 0; otherwise, the risks of eddy jumping and eddy missing are too great.  
478 The look-ahead approach effectively reduces such risks. For example,  $N=1$  and  $N=2$  have 95.5% and 98% of the  
479 total eddies for  $N=4$ , respectively. To reduce the missing eddies to 1%, the look-ahead time might be greater than six  
480 days. This is also the physical requirement of the representative period of the merged SLA data [Chelton et al.,  
481 2011b]. Although  $N=4$  might be better,  $N=2$  produced a very similar result (~2% bias to  $N=4$ ) and with a  
482 significantly lower computational cost. Our present parameters are reasonable considering of computational cost.

483 It should be pointed out that GEM is relatively independent to MEI, but the ratios  $r_1$ ,  $r_2$  and  $r_c$  might be sensitive to  
484 the method used in identification. We noted that [GEM based on Okubo–Weiss \(O–W\) parameter identification](#) ~~Θ–W~~  
485 ~~based identification~~ is much sensitive [to the critical value  \$r\_c\$](#)  than SLA based one, since O-W based eddies are much  
486 smaller and more possible to be unreal [Chaigneau et al., 2008]. Besides,  $r_c$  may not be independent with  $N$ , and the  
487 present  $r_c$  should only be valid for small time steps. If the time step is too large, the distance of eddy motion may be  
488 too far. And eddy snapshots can't overlap with each other. This constrain for time step is something like the  
489 Courant–Friedrichs–Lewy (CFL) condition (for time step) in computer fluid dynamics. In general, we think any  
490 tracking method should have this time-step limitation (depending on eddy size/propagation speed), if one don't want  
491 to mix one signal with another.

492 Finally, as noted in section 4.2, there are short-term eddies (lifetime < 30 days), which might [to though experience](#)  
493 complex evolution process. If only long-term eddies (lifetime > 30 days) were saved, the corresponding evolution  
494 process might not be recorded properly. This should be noted in further applications on eddy dynamics with satellite  
495 altimetry data.

### 496 5.3 Impact of eddy boundary

497 It is difficult to directly compare the influences of eddy boundary due to parameter choice in eddy identification. We  
498 can, however, estimate the influence of the eddy boundary using an indirect way. Because the eddy center is  
499 relatively robust, different identification methods mainly give different eddy boundaries. Consequently, the eddy  
500 area  $S$  is most sensitive to such an eddy area. However, the area ratio reduces the sensitivity to the eddy area  $S$   
501 because both the overlap area  $S_{12}$  and the eddy area  $S$  change synchronously. Moreover, our tracking results  
502 fortunately are not very sensitive to  $r_c$  (or the eddy area  $S$ ), as noted in the above discussion. For example, the  
503 present results are based on a very strict identification method. If we modify the threshold of eddy amplitude from 1  
504 cm to 3 cm, the number of identified eddies will decline. Nevertheless, the identification results for the long-lived  
505 eddies appear to be similar (Table 1).

506 However, such sensitive test may be only valid for the comparison of different parameter values in a same  
507 identification method. ~~It can't be simply extended to the comparison of varies identified eddies by different~~  
508 ~~identifications, since the eddy detection algorithms distinguish a lot with each other.~~ ~~comparison of eddies identified~~  
509 ~~by different methods, since the eddy detection algorithms differ a lot from each other.~~ -In general, the automated  
510 eddy detection algorithms are categorized into three types: 1) physical parameter-based algorithms, e.g., Okubo-  
511 Weiss (O-W) parameter [Isern-Fontanet et al., 2003; Chaigneau et al., 2008]; 2) flow geometry-based algorithms  
512 [Chaigneau et al., 2011; Chelton et al., 2011b; Wang et al., 2015]; and 3) hybrid methods, which involve physical  
513 parameters and flow geometry characteristics [Nencioli et al., 2010; Xiu et al., 2010; Dong et al., 2011; Yi et al.,  
514 2015]. For example, Yi et al. (2015) used the O-W parameter to identify eddy kernels and SLA contour geometries  
515 to identify eddy boundaries. So it is difficult to compare the influences of eddy territory by using different  
516 identification and tracking algorithms.

517

### 518 5.4 Future research

519 The GEM is a flexible model that can easily work with other relevant programs, e.g., data filtering and smoothing  
520 algorithms [Chelton et al., 2011b; Ienna et al., 2014; Wang et al., 2014], other hybrid eddy detection algorithms [e.g.,  
521 Yi et al., 2015] and O-W parameter detection [e.g., Petersen et al., 2013], because the GEM only requires a flow  
522 field and previously identified eddies to accomplish dynamic tracking. In addition, the similarity measurement can  
523 be replaced by similar methods [e.g., Pegliasco et al., 2015] when considering more complex conditions.

524 The identified eddies by using other identification algorithm without watershed can also be tracked with the GEM.  
525 In this case, the strong interaction stage of eddies “in conjunction”, which leads to genesis and termination of eddies,  
526 is more likely missed as pointed out in section 2.3. However, the weak interaction stage of eddies (watershed free) in  
527 some far distance could still be recorded, because most of merging/splitting records occurred at the interaction of  
528 two eddies with a certain distance. This weak interaction still can't be recorded by previously interaction-free

529 tracking algorithm, which records only the isolated tracks. Thus the GEM extends the potential applications of  
530 previously identified eddies.

531 The GEM is a complex model. The output data include eddy tracks, relationships and previously identified eddy  
532 characteristics (e.g., amplitude and radius). These eddy characteristics, which were directly obtained from the  
533 identification process, are useful for censuses [Chelton et al., 2011b]. However, they may not be sufficiently  
534 accurate for some applications. For example, eddy area was required in our recent studies on typhoons and oceanic  
535 eddy interactions [Sun et al., 2010, 2012, 2014]. Besides, some physical quantity (circulation, angular momentum,  
536 energy) are required to be accurately calculated in the investigation of eddy dynamics process. A better way to  
537 obtain these characteristics might be to use a nonlinear fitting of the flow field [Wang et al., 2015; Yi et al., 2015]  
538 with appropriate models [e.g., Sun, 2011; Zhang et al., 2013] other than simply estimated from identification.

539 Another future research direction may involve comparing different tracking datasets. Because there are several  
540 tracking datasets produced by various methods, it is useful to inter-compare them. This may improve both the  
541 tracking methods and the available datasets for further studies.

542 The GEM can be easily applied to larger datasets, even to 3-D numerical simulation outputs [Petersen et al., 2013;  
543 Woodring et al., 2016], because its computational time increases only linearly as a function of the size of the dataset.  
544 The computation of the 20-year daily global SLA data only required a few hours on a personal computer. In a  
545 personal computer with CPU of i7-6700k and 4.00 GHz, it takes about 15 minutes to identify snapshots of eddies,  
546 about 20 minutes to establish similarity, and about 10 minutes to track eddies in the North Pacific Ocean (NPO) with  
547  $0.25^\circ \times 0.25^\circ$  resolution of 20-year daily “DT14” data. Such a model can be used to analyze numerical simulation  
548 outputs.

549 The GEM opens a window to investigate eddy dynamics [Wang et al., 2015] and other applications [Sun et al., 2014]  
550 on those problems, e.g. (i) the strong eddy interaction which leads to genesis and termination of eddies (ii) the weak  
551 eddy interaction which associates with merging/splitting events (iii) the weak eddy interaction which modulates the  
552 eddy track and motion. As illuminated in Figure 11, the dynamic evolution of eddies is accompanied by abundant  
553 phenomena that might be identified using the GEM. The present study is only the beginning of such applications.

554

## 555 **6 Conclusions**

556 We have introduced the GEM for the tracking of the dynamic evolution of mesoscale eddies in the ocean. Several  
557 novel approaches (e.g., vector similarity and look-ahead approach) were applied to deal with unsolved problems in  
558 tracking. All of the computational steps in GEM are linear and do not require iteration. Given the grid number of the  
559 target region  $L$ , the maximum number of eddies  $M$ , the number of look-ahead time steps  $N$ , and the total time steps  $T$ ,  
560 the total **computational-time** complexity is of  $O(LM(N+1)T)$ . We applied the GEM to the eddies in the north Pacific.  
561 Eddy tracks were smooth because we required that the snapshots of eddies on neighboring days overlap one another.  
562 Both merging and splitting rates of eddies were high, especially at the western boundary, in strong currents and in

563 “eddy deserts”. The GEM is useful not only for satellite-based observational data but also for the output of  
564 numerical simulations. It potentially has many applications for studies of dynamic processes in related fields, e.g.,  
565 the dynamics of cyclones in meteorology. The “MEI” and “GEM” computer codes and program manual will be  
566 provided openly at the website [https://www.researchgate.net/profile/Liang\\_Sun20/](https://www.researchgate.net/profile/Liang_Sun20/) after publication of this  
567 paper.

568

569

### 570 **Acknowledgements**

571 | We thank the anonymous referees [and Dr. John M. Huthnance](#) for their comments and suggestions. We thank the  
572 AVISO for providing the SLA data (<http://www.aviso.oceanobs.com/>). This work was supported by the National  
573 Basic Research Program of China (Nos. 2012CB417402 and 2013CB430303), the National Foundation of Natural  
574 Science (No. 41376017) and the Open Fund of the State Key Laboratory of Satellite Ocean Environment Dynamics  
575 (No. SOED1501).  
576

577 **References**

- 578 Batchelor, G. K. (2000). *An introduction to fluid dynamics*. Cambridge university press, 615pp.
- 579 Bennett, A. F., & White, W. B. (1986). Eddy heat flux in the subtropical North Pacific. *J. Phys. Oceanogr.*, 16(4),  
580 728-740.
- 581 Capet, A., E. Mason, V. Rossi, C. Troupin, Y. Fauge`re, I. Pujol, and A. Pascual, (2014), Implications of refined  
582 altimetry on estimates of mesoscale activity and eddy-driven offshore transport in the Eastern Boundary Upwelling  
583 Systems, *Geophys. Res. Lett.*, 41, 7602–7610, doi:10.1002/2014GL061770.
- 584 Carrere, L., Faugère, Y., and Ablain, M. (2016). Major improvement of altimetry sea level estimations using  
585 pressure-derived corrections based on ERA-Interim atmospheric reanalysis, *Ocean Sci.*, 12, 825-842,  
586 doi:10.5194/os-12-825-2016.
- 587 Chaigneau, A., Gizolme, A., and Grados, C. (2008). Mesoscale eddies off Peru in altimeter records: identification  
588 algorithms and eddy spatio-temporal patterns. *Progr. Oceanogr.*, 79, 106–119.
- 589 Chaigneau, A., Le Texier, M., Eldin, G., Grados, C., and Pizarro, O. (2011). Vertical structure of mesoscale eddies  
590 in the eastern South Pacific Ocean: A composite analysis from altimetry and Argo profiling floats, *J. Geophys. Res.:*  
591 *Oceans*, 116. C11025, doi:10.1029/2011JC007134.
- 592 Chelton, D.B., Schlax, M.G. (1996). Global observations of oceanic Rossby waves. *Science* 272, 234–238.
- 593 Chelton, D. B., Schlax, M. G., Samelson, R. M., & de Szoeke, R. A. (2007). Global observations of large oceanic  
594 eddies. *Geophys. Res. Lett.*, 34(15), L15606. doi:10.1029/2007GL030812.
- 595 Chelton, D. B., Gaube, P., Schlax, M. G., Early, J. J., & Samelson, R. M. (2011a). The influence of nonlinear  
596 mesoscale eddies on near-surface oceanic chlorophyll. *Science*, 334(6054), 328-332.
- 597 Chelton, D. B., Schlax, M. G., & Samelson, R. M. (2011b). Global observations of nonlinear mesoscale eddies.  
598 *Progr. Oceanogr.*, 91(2), 167-216.
- 599 Dong, C., Nencioli, F., Liu, Y., & McWilliams, J. C. (2011). An automated approach to detect oceanic eddies from  
600 satellite remotely sensed sea surface temperature data. *Geoscience and Remote Sensing Letters, IEEE*, 8(6), 1055-  
601 1059.
- 602 Dong, C., McWilliams, J. C., Liu, Y., & Chen, D. (2014). Global heat and salt transports by eddy movement. *Nature*  
603 *communications*, 5:3294, DOI: 10.1038/ncomms4294.
- 604 Duacs/AVISO (2014), A new version of SSALTO/Duacs products available in April 2014. Version 1.1, CNES.  
605 [Available at [http://www.avisio.altimetry.fr/fileadmin/documents/data/duacs/ Duacs2014.pdf](http://www.avisio.altimetry.fr/fileadmin/documents/data/duacs/Duacs2014.pdf)].
- 606 Fang, F., and Morrow, R. (2003). Evolution, movement and decay of warm-core Leeuwin Current eddies. *Deep-Sea*  
607 *Res., Part II* 50, 2245–2261.

608 Fujiwhara, S. (1921). "The natural tendency towards symmetry of motion and its application as a principle in  
609 meteorology". *Q. J. R. Met. S.* 47 (200): 287–293. doi:10.1002/qj.49704720010.

610 Faghmous, J. H., Uluyol, M., Styles, L., Le, M., Mithal, V., Boriah, S., & Kumar, V. (2013). Multiple Hypothesis  
611 Object Tracking For Unsupervised Self-Learning: An Ocean Eddy Tracking Application. In AAAI.

612 Hu, D., Wu, L., Cai, W., Gupta, A. S., Ganachaud, A., Qiu, B. ... & Wang, G. (2015). Pacific western boundary  
613 currents and their roles in climate. *Nature*, 522(7556), 299-308.

614 Ienna, F., Jo, Y. H., & Yan, X. H. (2014). A new method for tracking Meddies by satellite altimetry. *Journal of*  
615 *Atmospheric and Oceanic Technology*, 31(6), 1434-1445.

616 Isern-Fontanet, J., García-Ladona, E., & Font, J. (2003). Identification of marine eddies from altimetric maps.  
617 *Journal of Atmospheric and Oceanic Technology*, 20(5), 772-778.

618 Li, Q. Y., Sun, L., Liu, S. S., Xian, T., & Yan, Y. F. (2014). A new mononuclear eddy identification method with  
619 simple splitting strategies. *Remote Sensing Letters*, 5(1), 65-72. doi:10.1080/2150704X.2013.872814.

620 Li, Q. Y., & Sun, L. (2015). Technical Note: Watershed strategy for oceanic mesoscale eddy splitting. *Ocean*  
621 *Science*, 11(2), 269-273. doi: 10.5194/os-11-269-2015.

622 Mason, E., Pascual, A., & McWilliams, J. C. (2014). A new sea surface height–based code for oceanic mesoscale  
623 eddy tracking. *Journal of Atmospheric and Oceanic Technology*, 31(5), 1181-1188.

624 McGillicuddy, D. J. (2011). Eddies masquerade as planetary waves. *science*, 334(6054), 318-319. doi:  
625 10.1126/science.1208892.

626 Nencioli, F., Dong, C., Dickey, T., Washburn, L., & McWilliams, J. C. (2010). A vector geometry-based eddy  
627 detection algorithm and its application to a high-resolution numerical model product and high-frequency radar  
628 surface velocities in the Southern California Bight. *Journal of Atmospheric and Oceanic Technology*, 27(3), 564-579.

629 Penven, P., Echevin, V., Pasapera, J., Colas, F., and Tam, J.: Average circulation, seasonal cycle, and mesoscale  
630 dynamics of the Peru Current System: A modeling approach, *J. Geophys. Res.*, 110, C10021,  
631 doi:10.1029/2005jc002945, 2005.

632 Petersen, M. R., Williams, S. J., Maltrud, M. E., Hecht, M. W., & Hamann, B. (2013). A three-dimensional eddy  
633 census of a high-resolution global ocean simulation. *Journal of Geophysical Research: Oceans*, 118(4), 1759-1774.

634 Pegliasco, C., A. Chaigneau, and R. Morrow, (2015). Main eddy vertical structures observed in the four major  
635 Eastern Boundary Upwelling Systems, *J. Geophys. Res. Oceans*, 120, 6008–6033, doi:10.1002/2015JC010950.

636 Sun L, Yang Y.-J., Xian T., Lu Z. and Fu Y.-F., (2010). Strong enhancement of chlorophyll a concentration by a  
637 weak typhoon, *Mar. Ecol. Prog. Ser.*, 404, 39-50, doi: 10.3354/meps08477.

638 Sun, L. (2011). A typhoon-like vortex solution of incompressible 3D inviscid flow. *Theoretical and Applied*  
639 *Mechanics Letters*, 1(4), 042003.

640 Sun, L., Yang, Y.-J., Xian, T., Wang, Y., and Fu, Y.-F., (2012). Ocean responses to Typhoon Namtheun explored  
641 with Argo floats and multiplatform satellites. *Atmos. Ocean*. 50(sup1), 15-26.

642 Sun, L., Y.-X. Li, Y.-J. Yang, Q. Wu, X.-T. Chen, Q.-Y. Li, Y.-B. Li, & T. Xian (2014). Effects of super typhoons  
643 on cyclonic ocean eddies in the western North Pacific: A satellite data-based evaluation between 2000 and 2008. *J.*  
644 *Geophys. Res. Oceans*, 119(9): 5585–5598, doi:10.1002/2013JC009575.

645 Wang, R., Yang, Z., Liu, L., Deng, J., & Chen, F. (2014). Decoupling noise and features via weighted L1-analysis  
646 compressed sensing. *ACM Transactions on Graphics (TOG)*, 33(2), 1-12.

647 Wang, Z., Li, Q., Sun, L., Li, S., Yang, Y., & Liu, S. (2015). The most typical shape of oceanic mesoscale eddies  
648 from global satellite sea level observations. *Frontiers of Earth Science*, 9(2), 202-208. doi: 10.1007/s11707-014-  
649 0478-z.

650 Woodring, J., Petersen, M., Schmeiber A., Patchett J., Ahrens J., Hagen H., (2016). In Situ Eddy Analysis in a High-  
651 Resolution Ocean Climate Model, *IEEE Transactions on Visualization & Computer Graphics*, 22(1), 857-866,  
652 doi:10.1109/TVCG.2015.2467411

653 Xiu, P., Chai, F., Shi, L., Xue, H., & Chao, Y. (2010). A census of eddy activities in the South China Sea during  
654 1993–2007. *Journal of Geophysical Research: Oceans*, 115(C3). C03012, doi:10.1029/2009JC005657

655 Xu, C., Shang, X. D., & Huang, R. X. (2011). Estimate of eddy energy generation/dissipation rate in the world  
656 ocean from altimetry data. *Ocean Dynamics*, 61(4), 525-541.

657 Yang, G., Wang, F., Li, Y., Lin, P., (2013). Mesoscale eddies in the northwestern subtropical Pacific Ocean:  
658 Statistical characteristics and three-dimensional structures. *Journal of Geophysical Research: Oceans*, 118(4): 1906–  
659 1923.

660 Yi, J., Du, Y., Zhou, C., Liang, F., & Yuan, M. (2015). Automatic Identification of Oceanic Multieddy Structures  
661 From Satellite Altimeter Datasets. *IEEE JSTARS*, 8(4): 1555-1563.

662 Zhai, X., Johnson, H. L., & Marshall, D. P. (2010). Significant sink of ocean-eddy energy near western boundaries.  
663 *Nature Geoscience*, 3(9), 608-612.

664 Zhang, C. H., Xi, X. L., Liu, S. T., et al. (2014). A mesoscale eddy detection method of specific intensity and scale  
665 from SSH image in the South China Sea and the Northwest Pacific. *Science China: Earth Sciences*, 57: 1897–1906,  
666 doi: 10.1007/s11430-014-4839-y.

667 Zhang, Z., Zhang, Y., Wang, W., & Huang, R. X. (2013). Universal structure of mesoscale eddies in the ocean.  
668 *Geophysical Research Letters*, 40(14), 3677-3681. doi: 10.1002/grl.50736.

669

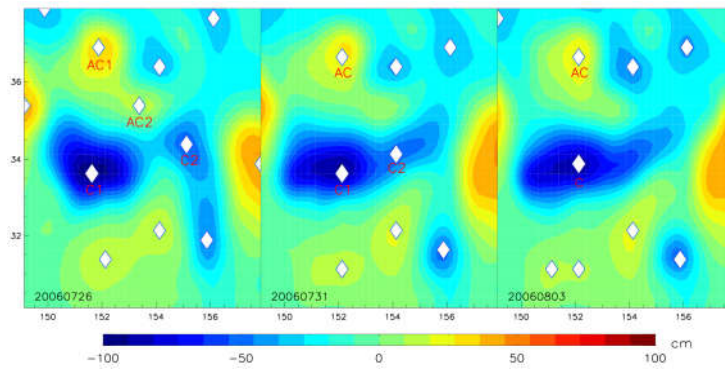
670



671 Table 1. The census of long-lived eddies, where “Amp” represents the amplitude threshold used in eddy detection;  
 672 and “C” and “AC,” respectively, represent cyclonic and anticyclonic eddies.

Amp	AC (>100 d)	C (>100 d)	AC (>400 d)	C (>400 d)
1 cm	7290	3627	198	22
3 cm	7118	3550	194	21

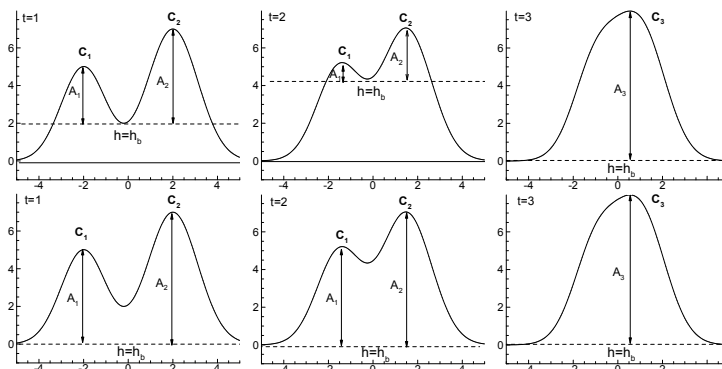
673



674

675 Figure 1. The evolutions of amplitudes and areas of eddies from July 5 to August 3, 2006 (after Li et al. 2014),  
 676 where the background field shows SLA, and white dots mark eddy centers. Two anticyclonic eddies AC1 and  
 677 AC2 merged into a single eddy on July 31, 2006. And, two cyclonic eddies C1 and C2 merged into a single one on  
 678 August 3, 2006.

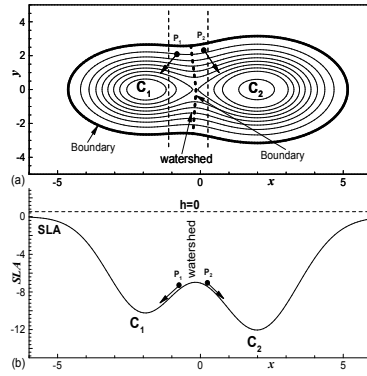
679



680

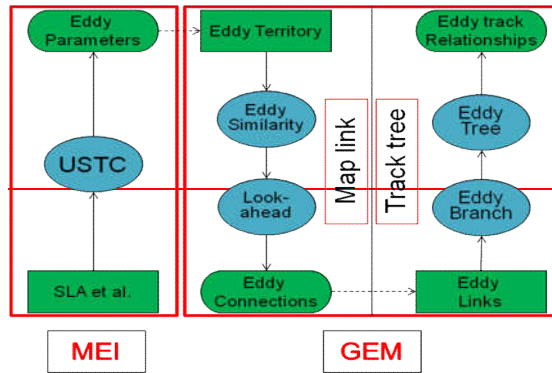
681 Figure 2. Top panels: Time evolution of two merging eddies revealed by the mononuclear eddy identification  
 682 without segmentation. Bottom panels: Time evolution of two merging eddies revealed by the mononuclear eddy

683 identification with segmentation. The  $h$  represents background SLA value,  $A$  represents amplitude of eddy,  
 684 and  $t$  represents the map at different time.

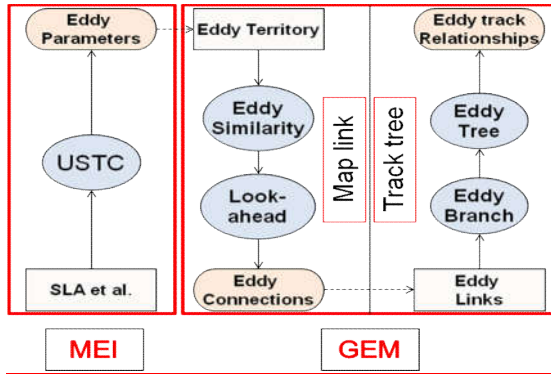


685  
 686 Figure 3. (a) Watershed as the natural division of eddies  $C_1$  and  $C_2$  from top view, where contours represent SLA. (b)  
 687 The particles  $P_1$  and  $P_2$  on the watershed flow downward to the eddy centres  $C_1$  and  $C_2$  from cross-section view.  
 688 After Li and Sun (2015).

689



690



691

692

693

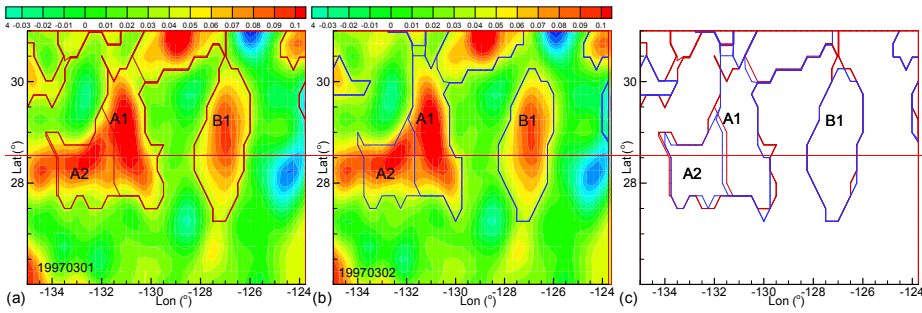
694

695

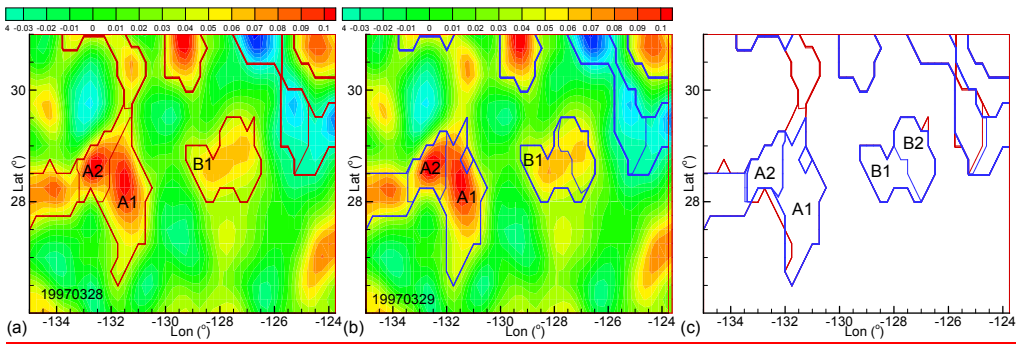
696

Figure 4. Flow chart of the systems. Mononuclear Eddy Identification (MEI) uses SLA to identify eddies via the Universal Splitting Technology for Circulations (USTC) method. The GEM, which has two independent parts of “Map link” and “Track tree”, then uses the previously identified eddies for tracking.

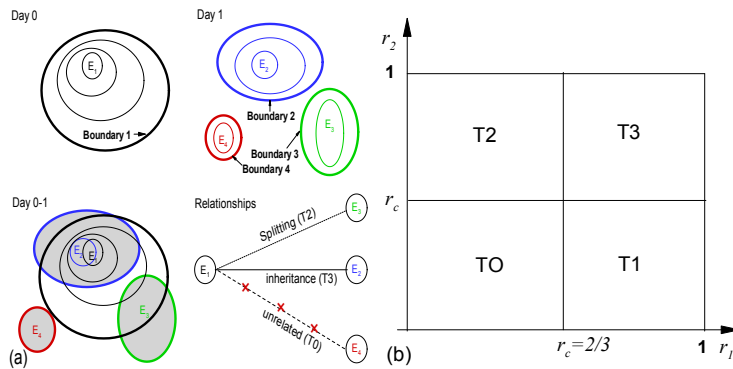
697



698



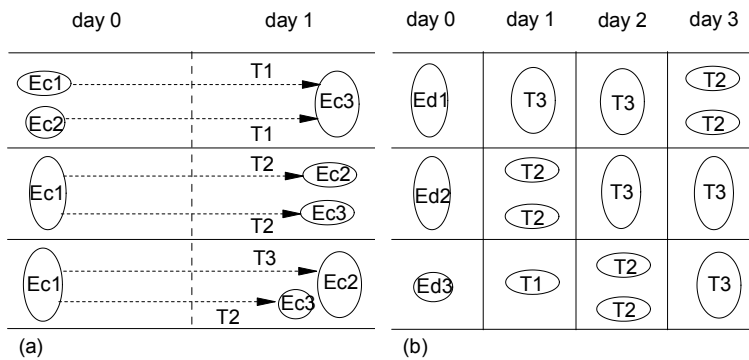
699 Figure 5. Sketch of eddy overlaps. (a) The SLA map (shading) and the boundary of eddies (red curves) on March 28,  
 700 1997, where A1, A2 and B1 represent identified eddies. (b) The SLA map (shading) and the boundary of eddies (blue  
 701 curves) on March 29, 1997. (c) The intersection of eddy territories areas by overlap eddy identification maps.  
 702



703  
 704 Figure 6. Sketch of eddy similarities. (a) The sketch of eddy overlaps. Eddy  $E_1$  (black) is the eddy identified on day  
 705 0, where the thin contours represent the eddy parameter (e.g., the SLA value). The thick contour represents the eddy  
 706 boundary. Eddies  $E_2$  (blue),  $E_3$  (green) and  $E_4$  (red) are identified on day 1. We consider the overlay between the two  
 707 eddies on different days to evaluate the similarity between them. (b) There are four similarity types (T0-T3)  
 708 according to the values of  $r_1$ ,  $r_2$  and the critical value  $r_c$ . there is at most one eddy that can be marked as a T1  
 709 (merging) or T3 (living) eddy on the following day.

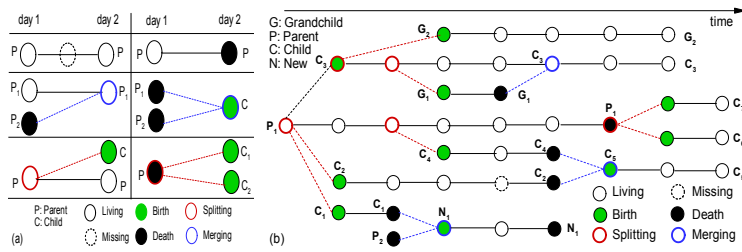
带格式的: 字体: 10 磅

710



711  
 712 Figure 7. (a) Three typical cases of successors (T1, T2 and T3) from one day (day 0) to another (day 1). (b) The  
 713 eddy at day 0 may have different successors corresponding to different numbers of "look-ahead" days, e.g., Ed1 at  
 714 day 0 may have a T3 eddy on day 2, and have two T2 eddies on day 3.

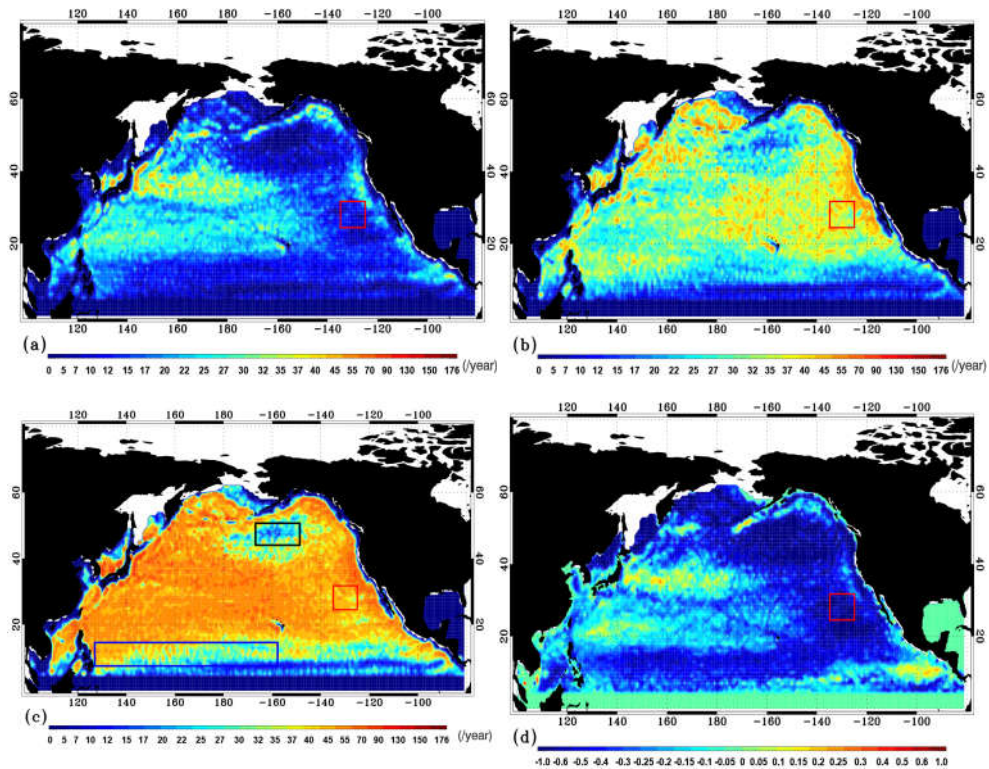
715



716

717 Figure 8. The logical genealogy of an ocean eddy with six states: birth, death, living, missing, splitting, and merging.  
 718 (a) The logical relationships of eddies between two days. (b) The logical genealogy evolution model of an example  
 719 eddy.

720



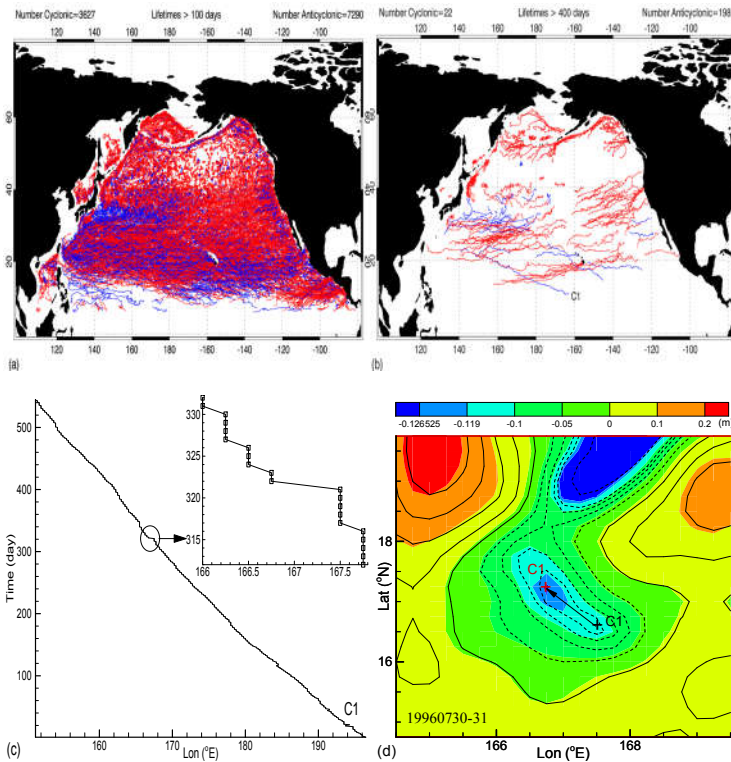
721

722

723 Figure 9 (a) The number of cyclonic eddy extrema on each  $1^{\circ} \times 1^{\circ}$  grid per year. (b) Same as (a), except for  
 724 anticyclonic eddies. (c) Same as (a), except for the total number of eddies. (d) The ratios of difference in number of

725 cyclonic and anticyclonic eddies to the total eddies (A logarithmic scale is used). The black box is the “eddy desert”,  
 726 the blue box is the NEC. The red boxes are the locations of merging/splitting examples in Figure 11, where  
 727 anticyclonic eddies dominated.  
 728

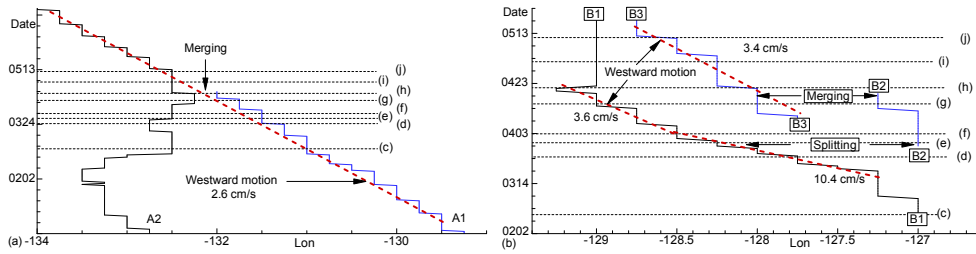
729



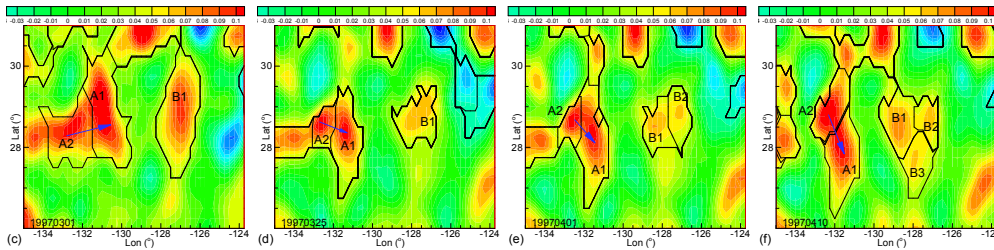
730

731 Figure 10. (a) Tracks of long-lived (>100 days) eddies. (b) Tracks of long-lived (>400 days) eddies. In (a) and (b),  
 732 blue color marks cyclonic eddies, and red color marks anticyclonic eddies. (c) The track of eddy C1. Note the  
 733 sudden jump from 167.5°E to 166.75°E on July 31, 1996. (d) The SLA fields on July 30 (contours) to 31 (shading),  
 734 using the same intervals for the contours and the shadings. The eddy centers are marked by a black cross (July 30)  
 735 and a red cross (July 31).  
 736

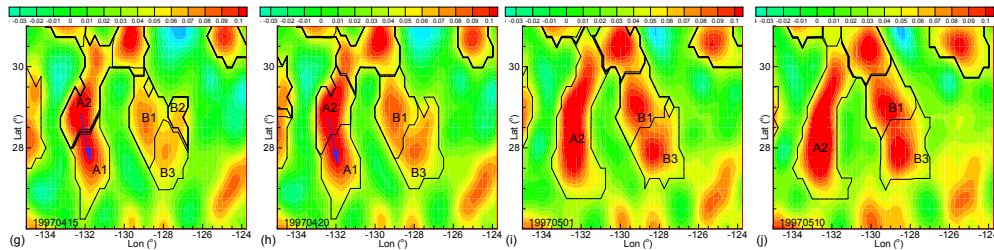
737



738



739



740

741

742

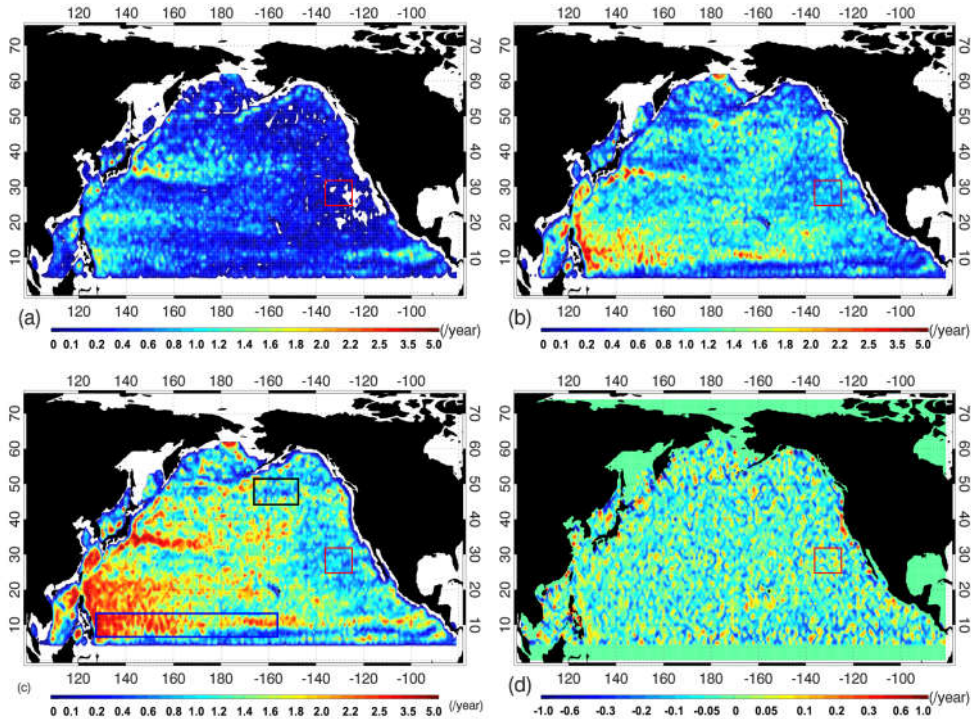
743

744

745

746

Figure 11. The dynamic evolutions of two groups of eddies, which are located in the red boxes in Fig. 9. (a) Two eddies, A1 and A2, approached each other, and A1 merged with eddy A2, where the blue arrows indicate that the eddy centers rotated clockwise during the merging process. (b) In the mean time, eddy B1 split into two small eddies. (c)-(j) The evolutions of SLA fields and eddies. Note that eddies A1 and A2 had clockwise rotations when they approached each other, as indicated by the blue arrows in (c)-(h).

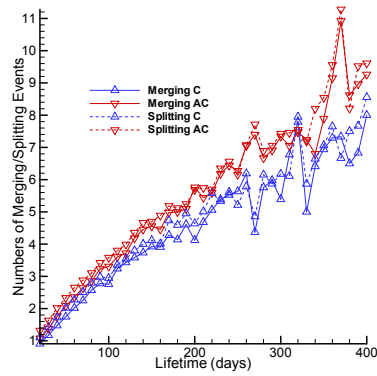


747

748

749 Figure 12. The frequencies of dynamic processes per  $1^{\circ} \times 1^{\circ}$  grid element. (a) The merging frequency for cyclonic eddies. (b) The merging frequency for anticyclonic eddies. (c) The merging frequency for all eddies. (d) The ratios of difference in number of cyclonic and anticyclonic eddies to the total eddies between the frequencies of merging  
 751 and splitting for all eddies to the sum of merging and splitting frequencies for all eddies. The boxes are the same in  
 752  
 753

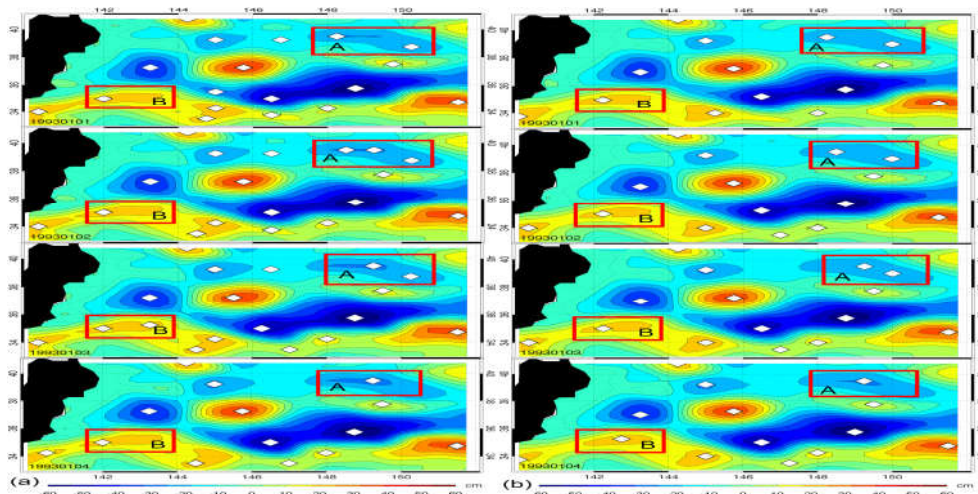
Figure 9. The blue box is the location of NEC, where merging frequency is high.



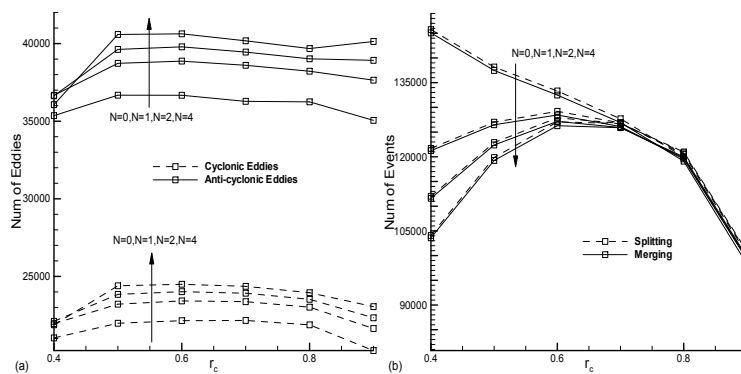
754



755 Figure 13. The number of merging/splitting events per eddy as function of eddy lifetime, where AC and C presents  
 756 anticyclonic and cyclonic eddies. The dynamic events are approximately linear increase with lifetime. The  
 757 merging/splitting events are more frequent for anticyclonic eddies than for cyclonic eddies.  
 758  
 759



760  
 761 Figure 14. Comparison of the non-smoothed (a) and smoothed SLA data (b) from January 1 to January 4, 1993,  
 762 where the color field shows SLA, white dots mark eddy centers, and two boxes A and B mark the regions sensitive  
 763 to noise. Note that small noises affected the eddy detection.  
 764



765  
 766 Figure 15. (a) Number of eddies (lifetime > 30 days) vs. the critical value  $r_c$  and look-ahead time  $N$ . (b) Number of  
 767 merging and splitting events vs. the critical value  $r_c$  and look-ahead time  $N$ .